8-2017

Exploring the Telecommunications Properties of the Human Nervous System: Analytical Modeling and Experimental Validation of Information Flow through the Somatosensory System

Natalie Hanisch
University of Nebraska-Lincoln, natalie.hanisch@huskers.unl.edu

EXPLORING THE TELECOMMUNICATIONS PROPERTIES OF THE HUMAN NERVOUS SYSTEM: ANALYTICAL MODELING AND EXPERIMENTAL VALIDATION OF INFORMATION FLOW THROUGH THE SOMATOSENSORY SYSTEM

by

Natalie Hanisch

A THESIS

Presented to the Faculty of

The Graduate College at the University of Nebraska

In Partial Fulfilment of Requirements

For the Degree of Master of Science

Major: Computer Science

Under the Supervision of Professor Massimiliano Pierobon

Lincoln, Nebraska

August, 2017

EXPLORING THE TELECOMMUNICATIONS PROPERTIES OF THE HUMAN NERVOUS SYSTEM: ANALYTICAL MODELING AND EXPERIMENTAL VALIDATION OF INFORMATION FLOW THROUGH THE SOMATOSENSORY SYSTEM

Natalie Hanisch, M.S.

University of Nebraska, 2017

Adviser: Massimiliano Pierobon

The growing field of Body Area Networks (BANs) is providing solutions to the wireless connectivity of wearable and implantable devices with applications in medicine, entertainment, fitness, and military, amongst others. While electromagnetic wave propagation has been the main BANs' enabling technology, the increasingly pervasive nature of these devices encourages novel solutions with added bio-compatibility and sustainability. In this thesis, a novel communication system is proposed for BANs based on the natural propagation of tactile stimuli through the nervous system. This system is composed of a tactile stimulator coupled to an ElectroEncephaloGraphy (EEG) system, and realizes the propagation of somatosensory signals from the index finger to the brain cortex. The feasibility of the proposed system is investigated through an experimental testbed, while an analytical modeling framework that captures the main processes at the basis of the proposed communication system is obtained by coupling computational models of somatosensory receptive fields with mathematical expressions of the cortical dynamics. Experimental results are then used to validate the ability of the proposed models to serve as fundamental tools for the design of systems based on tactile information transmission. In addition, digital modulation schemes, i.e., On-Off Keying (OOK) and Differential Pulse Position Modulation (DPPM), are

evaluated as potential strategies to transmit information through the proposed system. These preliminary contributions stand as proof-of-concept for the engineering of nervous-system-enabled BANs.

ACKNOWLEDGMENTS

Ancient Polynesians are considered to be some of the most talented wayfinders of the ocean. They were known to be able to travel long distances across open waters with no navigational equipment beyond their mind and senses. In my research, I like to imagine that observing the signals of the nervous system shares a complexity similar to that of the waves of the ocean. When I arrived at UNL, I felt lost in the stormy waters of decoding the natural signals of the nervous system. It is now as I complete my Masters degree that I feel a capacity for wayfinding has developed within me. It is only with the support of the following people that this has been possible.

First off, I would like to thank my adviser Dr. Massimiliano Pierobon. With your diligent support and guidance my research has been able to flourish. In addition, thank you to my committee members: Dr. Byrav Ramamurthy and Dr. Jitender Deogun for your interest in my work and your time reviewing it.

Next I would like to thank Dr. Dennis Molfese and Noah Clayton at the Center for Brain, Biology, and Behavior for your assistance and guidance in working with EEG recording and analysis.

Further, I would like to thank everyone in the MBiTe Lab, but especially those I share an office with, Zahmeeth Sakkaff and Alireza Khodaei. Thank you for all your kindness and support, and knowing how to help me out when I need it the most.

I also would like to thank all of the friends and family who have been there for me through every stage of my development. I do believe that many people cannot reach their potential only due to a lack of the right support network, and so I thank you for being the support that has allowed me to reach toward the peaks of mine.

Finally, thank you to Vincent Schramer for providing me with endless support, love, and companionship.

Contents

List of Figures

List of Tables

Chapter 1

Introduction

Body Area Networks (BANs) are based on cutting-edge communication technologies for the interconnection of devices on, in, or around the human body for a variety of possible uses, including medical, entertainment, fitness, and defense [36, 26, 1, 54]. The latest wearable and implantable devices are pushing the limits of these technologies by providing ubiquitous sensing of human body parameters and actuation capabilities coupled with enhanced biocompatibility and ergonomics [49, 4]. As the number of devices in the Internet of Bio-Nano Things (IoBNT) continues to expand, so does the demand for more efficient and effective interconnection techniques for BANs. While most research efforts around BANs [36] have been focusing on electromagnetic (EM) wireless technology and the propagation of EM waves around the body, as expressed in the standard IEEE 802.15.6 [1], technologies able to propagate information inside the body, or Intra Body Communication (IBC) [50], such as ultrasound [47], and galvanic coupling [29], are limited in their applicability, especially due to their invasiveness and unnatural characteristics, which could lead to negative effects on health [3].

Although IBC solutions based opto-ultrasonic communications [48] and Terahertz

band communications [2] have been proposed as possible alternatives to reduce the aforementioned invasiveness through the use of nanoscale communication devices and very short-range EM technologies, a potentially transformative direction stands in the utilization of biochemical processes already at the basis of natural communications inside our body [32, 3]. Despite the significant amount of research focused on networking for BANs, the specific approach of using the nervous system for transmission is an almost entirely untapped. [3]

In particular, the study of the nervous system and its neurons as a means to propagate information between future wearable and implantable devices is encouraged by its ubiquitous distribution within the body and the existence of well-established techniques for external interfacing, such as [17, 35]. To realize this goal, novel interdisciplinary research at the frontier of communication engineering and neuroscience is needed to develop communication theoretic tools and models that could exploit the wealth of knowledge built in recent years around modeling the physiological processes in the nervous system.

Most of the previous literature in this direction from the communication engineering community has mainly focused on the propagation of information in single or interconnected networks of neurons [6, 53], without addressing the context of the nervous system in the human body as a whole. While in [7, 10] detailed models are presented to study the natural propagation of neuro-spikes (or action potentials) in and between single neurons, in [27, 28] the authors explore the possibility of transmitting artificial (non-natural) information through a neuron without active generation of action potentials, through the use of the so-called subthreshold electrical stimulation. Other notable works in the literature are focused on the analysis of future techniques to enable intra-body neuron stimulation of electrochemical spikes through implantable nanotechnology-enabled devices [34].

1.1 Background and Motivation

While other approaches to IBC implementations generally focus on propagation of EM waves through the body, we propose a method that relies on the utilization of already present information pathways and the natural responses that drive this information transmission. Consider the following analogy: in the 1990s a dial-up Internet connection allowed access the World Wide Web, but but did not allow for simultaneous use of that same line for telephone calls. This was, as is well known, because the dial-up service used the same frequency range and technologies as was used for making a phone call. In the late 1990s and early 2000s, Digital Subscriber Lines (DSL) became broadly accessible, and it became possible to make a phone call while using the Internet. In this thesis we consider an analogous problem: when considering the human nervous system as an already present communication network, we explore the feasibility of using those same lines that regularly transmit natural information to also transmit artificial information throughout the body.

The nervous system is a collection of electrical wires that span throughout the entire body and connect the brain, sensory systems, and organs to each other. Not only is this natural communication network distributed throughout the entire human body, but it is also easily accessible. Every time you feel a sensation and every time you move a muscle, information is being transmitted through this natural system. Every time you think to make a movement, a signal is sent from the brain back through the body. This system is asymmetric. That is, if we consider the point-to-point communication between the surface of the skin and the brain, different processes need to occur for information to go from the skin to the brain than need to occur for the reverse direction of information transmission. We consider the forward-direction as the focus of this thesis, while the reverse direction will be the subject of future

work.

1.2 Contributions

We propose a communication system based on the propagation of tactile stimuli through the nervous system and its components. In short, we can transmit information by initiating a tactile sensation on the skin. This sensation generates an electrochemical impulse which propagates along the nerves of the somatosensory system and it is then received by the brain. The signal's arrival in the brain results in activity in the somatosensory cortex. Finally, this activity can be read through an ElectroEncephaloGraphy (EEG) device, and the received signal cleaned and processed to reveal the initial sensation pattern.

The contributions of this thesis are as follows:

1. We develop and implement an accurate analytical model that represents the transmission of artificial data through the human body.

2. We consider Differential Pulse-Position Modulation (DPPM) as a form of digital modulation and describe its advantages for this system.

3. We show that the analytical and experimental performance of the system are in agreement.

In a traditional communication system the message is transformed into an electrical signal by an encoder device, and in optical systems the message is translated into a light signal, in our system we can only modulate the signal by use of the timing and pressure of skin taps. The non-invasive nature and the availability of well-established techniques for EEG signal acquisition and analysis, as well as previous neuroscience literature on the modeling of somatosensory system processes, makes our proposed

system ideal to study for the development of IBC networks. In particular, in this thesis we develop an analytical modeling framework based on computational neuroscience models of the somatosensory signal propagation [16, 15] the somatosensory cortex at the brain [11], and the generation of EEG signals [38, 5].

At the same time, we present an experimental study performed through an ad-hoc experimental testbed, which is also used to validate the ability of the proposed analytical models to serve as fundamental tools for the design of systems based on haptic information transmission. Some similarities with this approach can be found in very recent literature [51, 19], where the cortex representation resulting from Braille tactile stimulation through the somatosensory system is studied by analyzing the EEG. In [51] the EEG response to mechanical Braille stimulation is analyzed in order to later compare to the neural response from electronic Braille stimulation.

Nevertheless, these studies do not aim at building analytical models, and are not placed in the context of IBC engineering. The latter applies also to [55] where a conceptual network model of each signal transduction step in human nervous system from a sensory neuron to brain astrocytes is detailed, but this model does not include an overall model of touch receptive fields and the cortex, nor the signal reception through EEG. Although an attempt has been made to model the overall touch propagation through the somatosensory system in [45], this paper does not include numerical data, nor experimental data or validation of the presented models, which are based on finite state machines rather than physiological models from neuroscience.

This thesis is organized as follows. In Chapter 2 we provide a high-level description of the system and its key components. In Chapter 3 we detail the implementation of an *in-vivo* experimental test bed for this system. In Chapter 4 we detail our analytical model of the system and provide key implementation details. In Chapter 6 we provide the results of experiments developed by the experimental and analytical

implementations. In Chapter 7 we conclude and discuss future research directions.

Chapter 2

Description of the Proposed System

Our system, which is based on the idea of transmitting artificial data through the natural pathways of the human nervous system, is comprised of three primary components:

1. The **Transmitter**, which which encodes information into a somatosensory signal through tactile stimulation of the skin.

2. The **Channel**, which is made up of nerve pathways that propagate the signal to the somatosensory cortex of the brain.

3. The **Receiver**, which is an EEG device used to record the neural activity in the somatosensory cortex after a signal is transmitted.

It is useful to note that for this work we focused on one-way data transmission from the right index finger to the somatosensory cortex. This is because our system is asymmetric in the sense that sending information from the surface of the skin to

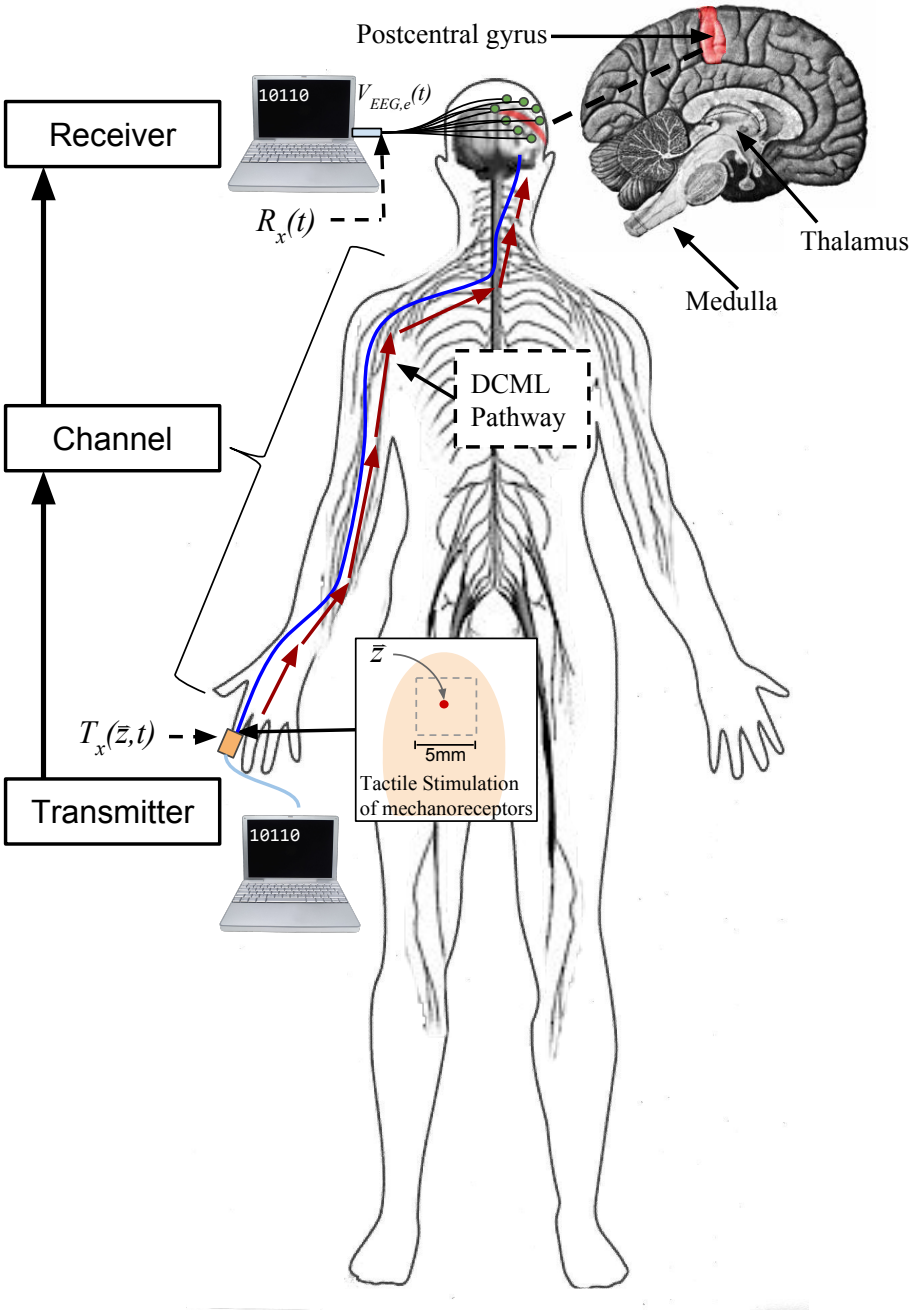

Figure 2.1: Schematic of the proposed communication system based on tactile information transmission.

an internal location is a different problem than transmitting data from an internal location back to the surface of the skin.

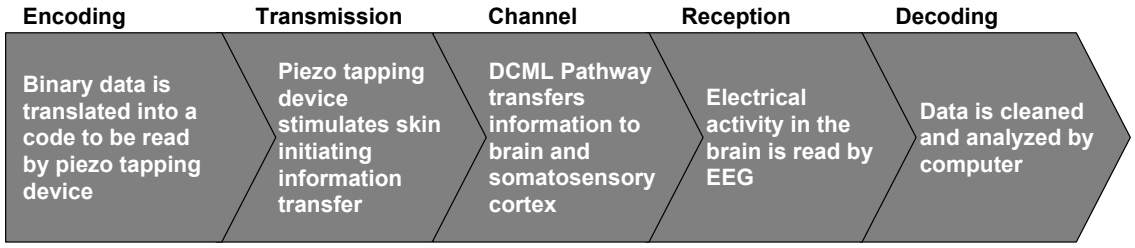

Figure 2.2: Block diagram of the proposed communication system.

Figure 2.1 provides a graphical sketch of the overall system, and Figure 2.2 provides a block diagram of the key system components. The transmitter consists of the computer modulating the taps, and the piezoelectric simulator which provides brief taps to a small ($\approx 1mm^2$) portion of the skin surface. This initiates the information transfer which travels along the nerves of the somatosensory system (explained in detail in the following sections) and then arrives at the brain. The receiver includes the EEG electrodes attached to the scalp record this activity in a localized area on the scalp and the computer which demodulates and decodes the transferred information. The following sections present a high-level overview of this system and its main components. The following two chapters discuss the experimental and analytical details of the system respectively.

2.1 The Transmitter

Information *bits* are encoded into a *somatosensory signal* by modulating the parameters of a **tactile stimulation** operated by a device. In our system, modulation is according to either On-Off Keying (OOK) or Differential Pulse Position Modulation (DPPM) provided in Chapter 5. To modulate the signal, the device controls the time instants t_0 and the duration T of skin taps at a precise location. Since each tap is realized by protruding a pin with a diameter of 2 mm, we approximate the tapping

location with a point on the skin surface. Within this thesis, we also assume that the tapping location is roughly at the center of the right index finger pad, denoted with the two-dimensional location coordinate $\vec{z}_{in}$, considered one of the most touch-sensitive skin locations of the human body [23]. The transmitted signal $T_x(\vec{z}, t)$, as function of the time t and the two-dimensional skin location $\vec{z}$, is expressed as follows:

$$T_x(\vec{z}, t) = \delta\left(|\vec{z} - \vec{z}_{in}|\right) A \,\mathrm{rect}\left(\frac{t - t_0}{T} - \frac{1}{2}\right), \tag{2.1}$$

where $\delta(.)$ and rect(.) are the Dirac delta and the rectangular function, respectively, A corresponds to the intensity of the tap, which is considered constant and equal to 1 within the scope of this thesis, as explained in the following, and $||\vec{z} - \vec{z}_{in}||$ is the Euclidian distance on the skin surface between a skin location $\vec{z}$ and the tapping location $\vec{z}_{in}$.

2.2 The Channel

As described in Sec. 2.1, for the signal produced by the transmitter to enter the channel, a tactile sensation is produced on a specific location on the skin. **Mechanoreceptors** present on the skin surface transduce a mechanical deflection at the finger pad into an electrochemical signal [23, 16].

This signal then enters the **Dorsal Column Medial Lemniscus (DCML) Pathway**, which includes neurons at the tips of the fingers all the way to the brain. Neurons are specialized cells which transmit impulses between each other to facilitate natural communication through the body. The DCML pathway is a major physiological pathway for transmitting sensory information in the body. It is an interconnection of three orders of neurons that relay this electrochemical signal to the

brain by propagating and regenerating the signal along their cell body projections, or axons [44].

Starting at the finger pad, this pathway continues up the arm past the shoulder, into the spinal cord. Then it ascends the posterior column of the cord until reaching the caudal portion of the brainstem, called the medulla. At the medulla, the first order neurons relay the propagated signal to the second order neurons through synapses, junctions between nerve cells where electrochemical signals are relayed through neurotransmitters diffusing in gaps between the two cell bodies. Neurotransmitters are chemical substances released by neurons to aid in the propagation of impulses between neurons. The second order neurons connect their axons to the thalamus, a central region of the brain where nerve fibers project out to the cerebral cortex in all directions, where they also cross the midline to the opposite side of the spinal cord with respect to their origin side, in a region of their axons called medial lemniscus. At the Ventral Posterior Lateral (VPL) nucleus region of the thalamus, a second set of synapses connect the incoming second order axons to the third order neurons. The third order axons relay the incoming electrochemical signals via a third set of synapses into cortical neurons located at the postcentral gyrus of the brain, which is a region in the upper side of the brain opposite (at the left side in this case) to the side of the tapping location. There is evidence that a localized tactile stimulation corresponds to a localized set of cortical neurons receiving the resulting signal in a point-to-point fashion, where different stimuli locations correspond to different signaling locations in the brain [37]. Table 2.1 details key time points in the journey of electrochemical signal as it travels through the DCML Pathway.

Table 2.1: Commonly observed average delays of the stimulus response at different DCML pathway locations

Time (ms)	**Event**
0	Stimulus occurs (tap)
9	Stimulus response at shoulder
13	— at fifth cervical spine
20	— at somatosensory cortex

2.3 The Receiver

Finally, the signal propagation along the cortical neurons stimulates correlated **somatosensory cortex** activity. Neurons in the somatosensory cortex may react with electrochemical excitatory and inhibitory responses to the signals incoming from the DCML pathway. That is, any given neuron in a network may be more or less likely to transmit its own nerve impulse depending on the excitatory or inhibitory activity, respectively, of neighboring neurons. These electrochemical responses of brain cortex neurons, organized into mini-columns and functional columns interconnected through thalamocortical and corticocortical networks [9], result into ionic currents flowing across the brain cortex that cause the emission of electromagnetic waves, which are subsequently received at the EEG electrodes [38].

The Receiver uses an **EEG system** with electrodes placed on the scalp at different locations to measure voltage fluctuations induced by the aforementioned ionic currents at the brain cortex [38]. We consider a number E of electrodes placed on the scalp at predetermined standard locations [25]. The voltage fluctuations read by each electrode are affected not only by the somatosensory cortex activity correlated to the input tap in (2.1), but also by other brain activities, such as those related to higher-level cognitive functions. We aim to recognize the voltage fluctuations induced by the aforementioned tap-related somatosensory cortex activity. For this, we utilize a standard technique for measuring **SomatoSensory Evoked Potentials**

(SSEPs) [39], where the voltage fluctuations from each electrode correlated to an event, *i.e.*, tapping, are preprocessed through averaging and filtering, resulting in the voltage signals $V_{\mathrm{EEG},e}(t)$, for each electrode e. In addition, we take into consideration only the electrodes around the postcentral gyrus region of the brain [18], denoted with the set $\mathcal{G}$, since, as also explained above, other electrodes will not be able to read SSEP voltage fluctuations from the tap. As a consequence, the received signal $R_x(t)$, as function of the time t, is defined as follows:

$$R_x(t) = \{V_{\mathrm{EEG},e}(t) | e \in \mathcal{G}\} \ . \tag{2.2}$$

In this communication system, we are interested in SSEP signals $V_{\mathrm{EEG},e}(t)$ minimally dependent from the particular characteristics and state of each individual's nervous system. Based on experimental evidence [39, 42], *the SSEP signals in* (2.2) *show an overall standard pattern across different experiment realizations within the first 100 ms from the occurrence of a tap, characterized by local maxima and minima around precise time instants.* These details are experimentally validated in Chapter 3 and then analytically modeled in Chapter 4. After the signal is received and preprocessed is it demodulated and decoded through a Support Vector Machine (SVM) based classifier as explained in Chapter 5.

Chapter 3

Experimental Study

In this chapter we describe the experimental framework used for testing the proposed communication system. Fig. 3.1 provides an overview of the primary elements of the experimental testbed. The main experimental elements include the Tactile Stimulator which attaches to the right index finger and the EEG System which collects the information the somatosensory signal after it has propagated through the nervous system. When the data has been recorded a computer records the preprocesses the data. We discuss these elements in detail in the following sections.

3.1 The Tactile Stimulator

The Tactile Stimulator is a custom made device, courtesy of Electrical Geodesics Incorporated (EGI), designed to induce computer-controlled discrete tactile stimulation impulses (taps) on the skin of a test subject, and concurrently send discrete Time-To-Live (TTL) signals to the EEG recording device. We placed one of the actuators shown in Fig. 3.1 in contact with the subject's right index finger pad. Upon an electrical command at t_0, as defined in Section 2.1, a plastic pin included in the actuator

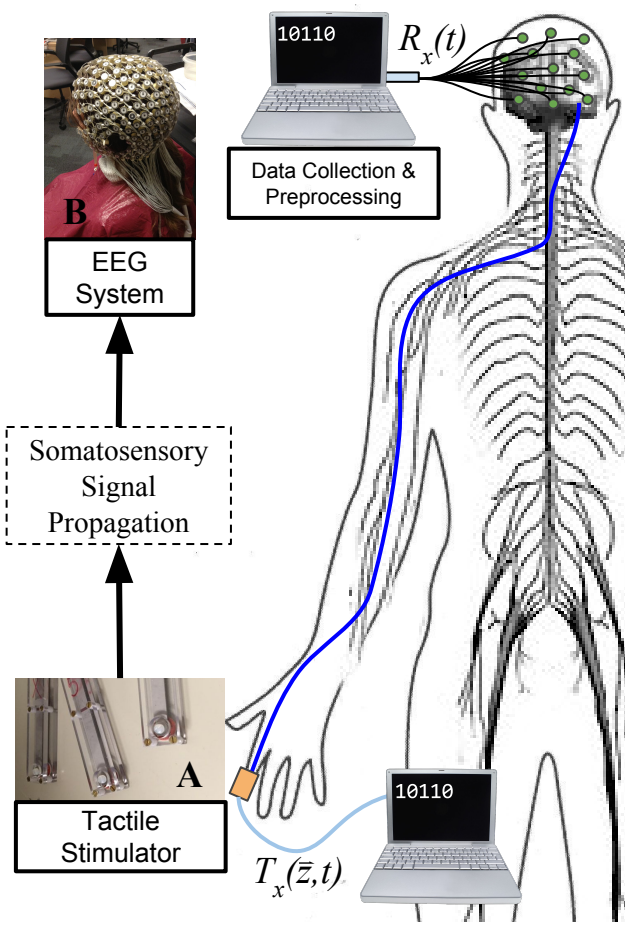

Figure 3.1: Schematic with the main components of the experimental framework for the proposed communication system.

moves upward and taps the skin. In our experiments, we secured the actuator to the finger making sure that the plastic pin would tap roughly at the center of the pad, which is in agreement with the value of the parameter $\vec{z}_{in}$ in Section 2.1 considered for the model-based simulation, as detailed in Chapter 4. This tactile stimulation device allows the control three parameters:

1. **Tap duration** (*i.e.* the period of time when the pin is in upward position and causes a skin deflection) which corresponds to the parameter T in (2.1).

2. **Frequency f_t of repetition** of these taps in a tapping sequence.

3. **Overall duration** T_s of the tapping sequence.

3.2 The EEG System

For the EEG data acquisition, we use a 256-channel HydroCel Geodesic Sensor Net®, shown in Fig. 3.1-B, connected to a Net Amps 300® amplifier, while the data have been recorded through the NetStation software (all EGI products) running on an Apple MacBook Pro laptop. This equipment was provided by the Center for Brain, Biology and Behavior (CB3). The 256 electrodes of the sensor net are immersed for 5 minutes in a saline solution containing 1.5 teaspoons of potassium-chloride warmed to body temperature. Following measurement and marking of the Fz and Cz (vertex) positions to aid in the alignment of the Net on the participant's head [30], the Net is placed on the head and impedances measured with Net Station 5.2 and, following common practice with high impedance systems, adjusted to under 60 kΩ prior to test commencement. The collected voltage reading from each of the 256 electrodes are digitized with a 24-bit A/D converter at a 1 KHz sampling rate.

3.3 Data Collection

The data analyzed in this paper was recorded on a single subject[1], right-handed female in her early 20s. The subject was comfortably seated in a quiet room, and the piezoelectric stimulator secured to her right index finger as described above. The tapping device was not audible, removing the possibility of cross-sensory contamination.

[1]The Institutional Review Board at the University of Nebraska-Lincoln has formally approved the disclosure of these data.

The tap duration T was set to 1 ms. For tapping repetition frequencies of $f_t = 1$Hz, $f_t = 10$Hz, and $f_t = 100$Hz, we run tapping sequences involving 5 seconds of stimulation followed by 5 seconds of rest. The goal of this stimulation was to capture the resulting SSEPs. In particular we want to understand how quickly we can transmit taps and overcome interference from brain activity associated with previous taps [39] and other physiological noise. We recorded SSEP data related to over $8,000$ taps in total.

3.4 EEG Data Preprocessing

For our preprocessing, and subsequent data analysis described in Chapter 6, we used the MATLAB toolbox EEGLAB, considered a standard computational tool in EEG data informatics [13]. Initially, the data was cleaned via visual inspection to remove any major artifact [14]. Next, the data was high-pass filtered at 0.1 Hz to remove amplitude shifts and other low frequency noise. For standard analysis of SSEPs in EEG, epoching, or chopping a continuous signal into a set of segments that are time-locked to a particular event is an important preprocessing step. The aforementioned data preparation was completed on all experimental data. Since post-experiment the data collected is essentially the same as that generated by the analytical model (described in Chapter 4), the final processing for generating these results in detailed in Chapter 6.

Chapter 4

Analytical Study

In this section, we present an analytical modeling framework which forms the basis of the mathematical expressions for the main processes involved in our communication system, as well as the implementation details. The following mathematical model was originally presented in our previous work [22]. As displayed in Fig. 4.1, this modeling framework is composed of four main analytical models, namely, the Finger Pad model, the DCML Pathway model, the Somatosensory Cortex model, and the EEG Generator model. The first two models are developed with reference to recent work in computational neuroscience [16, 15], where the authors build a computational model of the aforementioned cortical neuron reception of somatosensory signals upon tactile stimulation of the finger pad. The Somatosensory Cortex model is based on a formulation of the global theory of neocortical dynamics [11]. Finally, the EEG Generator model is inspired by the dipole neuron models studied in [38, 5], which provide mathematical expressions underlying the electromagnetic wave generating neural activity.

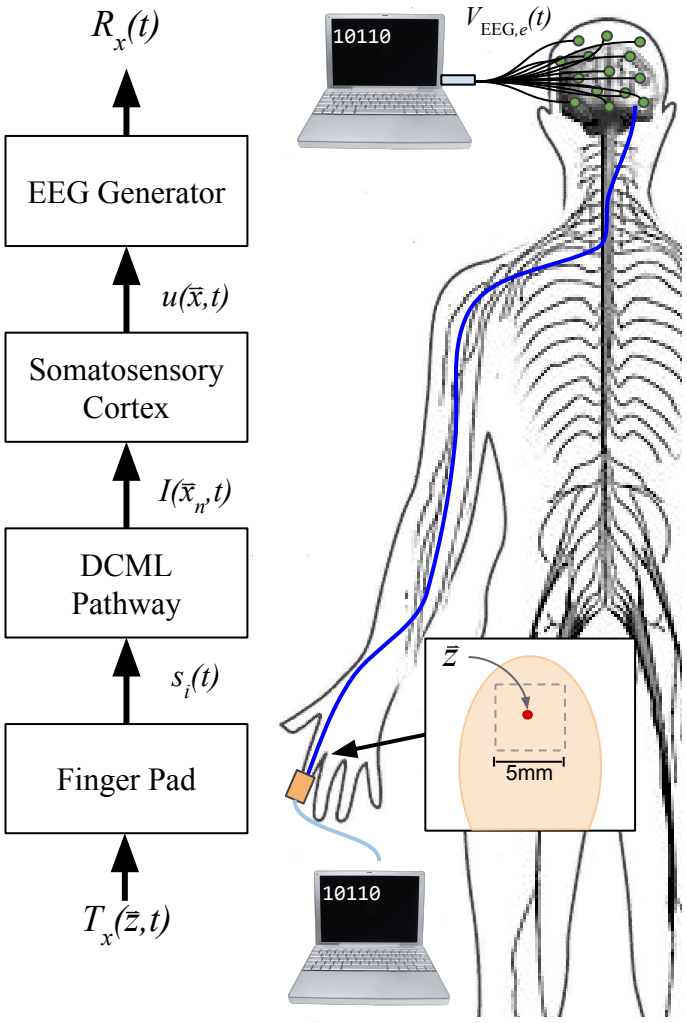

Figure 4.1: Schematic with the main models of the analytical framework for the proposed communication system.

4.1 The Finger Pad

Beginning at the finger pad, we consider a 5mm x 5mm patch of skin, with 256 receptors, and thus a receptor density of approximately 10 receptors/mm^2. This value was determined using Merkel's ending complex (MEC) density [41]. We let $a = 1$ and $\sigma = 1$ [16]. We consider $T = dt$, which is defined below, to reflect the same parameter value adopted in the experimental framework in Chapter 3. Finally, the

stimulus location $\vec{z} = [2.5\text{mm}, 2.5\text{mm}]$, which is the center of the finger pad.

The Finger Pad model converts the transmitted signal $T_x(\vec{z}, t)$ from (2.1) into the response $s_i(t)$ for each mechanoreceptor $i = 1, \ldots, \text{I}$ placed on the finger pad skin. With reference to [20], the response $s_i(t)$ can be approximated for any time t with a Gaussian function of the distance between the tapping location $\vec{z}_{in}$ and the location $\vec{z}_i$ of the mechanoreceptor i for the duration of the tap. This is computed from (2.1) with the following:

$$\begin{aligned} s_i(t) &= T_x(\vec{z}, t) * a \exp\left(-\frac{1}{2\sigma^2}|\vec{z} - \vec{z}_i|^2\right) \delta(t) \\ &= Aa \,\text{rect}\left(\frac{t - t_0}{T} - \frac{1}{2}\right) \exp\left(-\frac{1}{2\sigma^2}|\vec{z}_{in} - \vec{z}_i|^2\right), \end{aligned} \tag{4.1}$$

where $*$ denotes the convolution operation with respect to the time t, a and σ are the intensity of the mechanoreceptor response and the decay of the skin deflection with the distance from the tapping location, respectively, considered equal for every mechanoreceptor [20].

4.2 The DCML Pathway

The primary contribution of the DCML pathway is from the weights w_f^i which map the input from tactile stimulus on the skin to the corresponding patch of neurons in the somatosensory cortex. To obtain these weights, we used the source code and training procedure associated with [16], and available online at `https://github.com/gdetor/SI-RF-Structure` . Constants related to the weights are further explained in the next section as we utilized the same constants in training and simulation.

The DCML Pathway model takes the response $s_i(t)$ of each mechanoreceptor $i = 1, \ldots, \text{I}$ in input, and outputs the somatosensory signal $I(\vec{x}_n, t)$ that is received

by a neuron n at the two-dimensional location $\vec{x}_n$ in the brain cortex, as explained in Chapter 2. The index n identifies signal-receiving neurons, a total of N, present in a localized region of the postcentral gyrus, *i.e.*, the signaling location, also known as receptive field, that receives tactile stimuli from the right index finger pad [23]. With reference to [16, 15], the real DCML pathway behavior can be approximated by computing for each neuron n the average distance between receptor responses $s_i(t)$ and feedforward weights $w_f^i(\vec{x}_n)$ associated to the neuron itself. This model is expressed as follows:

$$I(\vec{x}_n, t) = 1 - \frac{1}{\mathrm{I}} \sum_{i=0}^{\mathrm{I}} \left| s_i(t) - w_f^i(\vec{x}_n) \right| . \tag{4.2}$$

While the relation in (4.2) expresses an instantaneous propagation from the mechanoreceptor responses to the somatosensory signals at the cortical neurons, in reality there is a propagation delay in the DCML pathway as the somatosensory signals go through the first, second, and third order of neurons and their synapses, as explained in Chapter 2. In the scope of this thesis, since the inclusion of a realistic model for the generation of this delay would imply the detailed knowledge of physiological parameters of each individual's nervous system, we limit ourselves to an empirical estimation through the experimental data.

4.3 The Somatosensory Cortex

In modeling the Somatosensory Cortex, we selected $dt = 1$ ms to reflect the sampling rate in our experimental setup (Chapter 3). We set $\tau, K_e, K_i, \sigma_e, \sigma_i$ to values used by [15] in their related model. The value v was based on the *characteristic velocity* of the brain cortex activity propagation in corticocortial fibers, according to [38]. The

cortical area was modeled with a 100x100 grid of 10,000 neurons, justified by the upper limit in the size of a cortical column [38]. A further justification for choosing this size of cortical area is that during the simulation of the model expressed in (4.3), we did not observe significant cortex activity after propagating for roughly 30 neurons outside of the receptive field. We modeled the receptive field of the right index finger pad at the center of this cortical area with a 32x32 grid of 1024 neurons, a number in agreement with [16]. As a consequence, each neuron n out of these 1024 is associated a location $\vec{x}_n$ and a set of feedforward weights $w_f^i(\vec{x}_n)$, one for every receptor on the skin patch. The remaining neurons in the modeled cortical area not part of the receptive field, and do not have feedforward weights. The purpose of these neurons is to allow the response signal to propagate through the cortical medium. We choose a toric distance measure to compute $|\vec{x} - \vec{y}|$ in (4.3) and (4.4), as suggested in [11].

The Somatosensory Cortex model computes the somatosensory cortex activity $u(\vec{x}, t)$ at each two-dimensional location $\vec{x}$ within the left postcentral gyrus of the brain at time t from the somatosensory signal $I(\vec{x}_n, t)$ received by the each neuron at location $\vec{x}_n$ within the aforementioned right index finger pad receptive field, function of the time t. According to the neural field model of the neocortical dynamics (see Appendix A), this computation can be approximated through the Nunez-Amari integro-differential equation [16, 15], and it is expressed as follows:

$$\begin{aligned}\tau \frac{\partial u(\vec{x}, t)}{\partial t} = & - u(\vec{x}, t) + \int_{\Gamma} w_l(\vec{x}, \vec{y}) f\left(u\left(\vec{y}, t - \frac{|\vec{x} - \vec{y}|}{v}\right)\right) d\vec{y} \\ & + I(\vec{x}_n, t)\delta(|\vec{x} - \vec{x}_n|)\,, \end{aligned} \tag{4.3}$$

where τ is the membrane time constant, v is the speed of propagation of cortex activity between neighboring neurons, Γ is the set of two dimensional coordinates included in the postcentral gyrus, $w_l(\vec{x}, \vec{y})$ is the lateral connection function between two neurons

located at $\vec{x}$ and $\vec{y}$, respectively, and $f(u(\vec{x},t))$ is the firing rate, as function of the cortex activity u at location $\vec{x}$ in the postcentral gyrus, and time t.

The lateral connection function $w_l(\vec{x},\vec{y})$ expresses the interplay between excitatory neurons, which respond to neighboring neuron activities with a positive signal, and inhibitory neurons, which respond to the same activities with a negative signal. The neural field theory (see Appendix A) and the Nunez-Amari equation model cortex activity as a continuum on the cortex surface, and excitatory and inhibitory neurons are modeled as part of a homogeneous mixed population [11], resulting in the following expression:

$$w_l(\vec{x},\vec{y}) = K_e \exp\left(-\frac{1}{2\sigma_e^2}|\vec{x}-\vec{y}|^2\right) - K_i \exp\left(-\frac{1}{2\sigma_i^2}|\vec{x}-\vec{y}|^2\right) \tag{4.4}$$

where K_e and K_i quantify the strength of excitation and inhibition of a neuron, respectively, and σ_e and σ_i express the intensity of excitation and inhibition, respectively, as function of the distance between two neurons. Commonly, (4.4) models the experimentally observed short range excitation and long range inhibition, which results in the condition $\sigma_i \gg \sigma_e$ [16].

The firing rate $f(u(\vec{y}, t-|\vec{x}-\vec{y}|/v))$ models the non-linear behavior underlying the excitability of a cortex neuron at location $\vec{y}$. This is usually expressed through a sigmoidal function of the cortex activity propagated at location $\vec{y}$ from location $\vec{x}$ at time t with velocity v [11]. For simplicity, as suggested in [21], we approximate the firing rate function f as follows:

$$f(u) = \begin{cases} u & u \geq 0 \\ 0 & u < 0\,. \end{cases} \tag{4.5}$$

4.4 The EEG Generator

The EEG generator model takes as input the somatosensory cortex activity $u(\vec{x}, t)$ at each location $\vec{x}$ within the left postcentral gyrus as function of the time t, and returns as output the received signal $R_x(t)$ expressed in (2.2). In agreement with [38, 5], from the point of view of the aforementioned generation of electromagnetic waves by ionic currents associated to the neocortex activity, and the consequent voltage recorded at the EEG electrodes, the somatosensory cortex can be modeled as a two-dimensional layer of electromagnetic-wave-emitting dipoles. In this model, the EEG electrodes are approximated as point-wise locations immersed in the conductive medium of the scalp, to which they are electrically connected through an electrolytic saline solution, gel, or paste [30]. As a consequence, in agreement with [5], the voltage signals $V_{\mathrm{EEG},e}(t)$ read by the electrode e as function of the time t can be expressed as

$$V_{\mathrm{EEG},e}(t) = \frac{\sigma_{in}}{4\pi\sigma_{ex}} \int_{\mathrm{surf}} k_v u(\mathbf{P}\vec{r}, t) d\Omega(\vec{r} - \vec{r_e}) \,, \tag{4.6}$$

where σ_{in} and σ_{ex} are the intracellular and extracellular conductivity, respectively, $\mathbf{P}$ is the orthogonal projection matrix equal to $[100; 010; 000]$ [8], $\mathbf{P}\vec{r}$ projects the three-dimensional coordinate $\vec{r}$ into the two-dimensional coordinate $\vec{x}$ of the somatosensory cortex, and $d\Omega(\vec{r} - \vec{r_e})$ is the solid angle that an infinitesimal surface unit (surface differential) subtends at the three-dimensional location $\vec{r_e}$ of the EEG electrode e [5]. We take $\sigma_{in} = \sigma_{ex} = 1$ S/mm [5]. Finally, k_v was estimated computationally based on the experimental results as detailed in Sec. 6.2. The simulated locations of the electrodes on the scalp is in agreement with the standard in [25], in the specific case where 256 electrodes are used. The constant parameter k_v converts the somatosensory cortex activity into a proportional electrical potential of the cell membrane of the cortex neurons at the same location and time. Within the scope of this thesis,

Table 4.1: Mathematical Notations

$\vec{z}$	Location on skin
$\vec{z_{in}}$	Tap location on skin
$\vec{z_i}$	Location of cutaneous receptor
t_0	Time instant of tap
$\mathcal{G}$	Set of EEG electrodes
$\vec{x_n}$	Two-dimensional neuron location
w_f^i	Feed-forward weights
$\mathbf{P}$	Orthogonal projection matrix
$\vec{r}$	Location in somatosensory cortex
$\vec{r_e}$	Location of EEG electrode

Table 4.2: List of Functions

T_x	Transmitted Signal
R_x	Received Signal
δ	Dirac Delta
$rect$	Rectangle Function
$V_{EEG,e}$	SSEP Signals
s_i	Receptor Response
I	Somatosensory input
w_l	Lateral Connections
f	Firing rate

we estimate the parameter k_v by scaling the received signal computed through the analytical model to that obtained from the experiments, as explained in Chapter 6.

4.5 Implementation

For the software implementation of our system, we consider the four main components and how they work together. For quick reference to values of constants, see Table 4.3. Algorithm 1 provides a high-level overview of the implementation of the aforementioned mathematical model.

Given a list of times at which stimulus should occur, for each numerical time value (spaced according to dt) in a specified time period ($[t_{start}, t_{stop}]$), if the current time

Table 4.3: Model Parameters

K_e	Excitation strength	3.65
K_i	Inhibition strength	0.1 mm
σ_e	Excitation intensity	2.40
σ_i	Inhibition intensity	1.0 mm
τ	Membrane time constant	1 s
dt	Time change	1 ms
T	Tap duration	1 ms
a	Intensity of response	1
σ	Decay of skin deflection	1
v	Cortical Propagation velocity	750 cm/s
σ_{in}	Intracellular conductivity	1 S/mm
σ_{ex}	Extracellular conductivity	1 S/mm
k_v	Proportionality constant	*est.* (see Chp.6)

value t is in the list-of-stimulus-times the Receptor Response s is generated based on the tap location x, otherwise the $s = 0$. From s the Neural Input is generated, this is essentially the implementation of (2.1) which is the mapping between a tap on the skin to the corresponding cortical response. The the Lateral Interactions (4.4) are generated based on the current cortical state u. Finally these values are brought together to determine the value for du as in (4.3), and then the cortical activity u is updated for the next time interval. Since the EEG signal at any time point is only dependent on the cortical state at that time point, the last two lines in the for-loop include calculating the solid angle formula for the current cortical state u, and then calculating the EEG response V.

Algorithm 1: Implementation of Analytical Model of Neural Response

Data: List of stimulus locations $\vec{z}$ and time $\vec{t}$

Result: Associated EEG response V

initialization;

for $t \in [t_{start}, t_{stop}]$ **do**

  if $t \in$ *list-of-stimulus-times* **then**

    $s = ReceptorResponse(x)$;

  else

    $s = 0$;

  end

  $I \leftarrow$ Neural-Input from s;

  $L \leftarrow$ Lateral-Interactions from u;

  Update du from dt, $u(t)$, L, I;

  $u(t+1) \leftarrow u(t) + du$;

  $V(t) \leftarrow$ EEG-Response from $u(t)$;

end

Chapter 5

Digital Modulation Techniques

Our system is limited in options for modulation because the main parameter that we can exploit for efficient modulation is the time instant at which a tactile stimulus is applied. This is in contrast to traditional communication systems which allow modulation though amplitude, phase, and frequency. As a result, our transmitter is more similar to an optical communications system than it is to an electric system. Within this thesis, we consider OOK and DPPM as modulation techniques for our system. This chapter discusses these modulation types in further detail, including their advantages and disadvantages with respect to our system. In addition this chapter covers the use of a Support Vector Machine (SVM) classifier to demodulate received EEG signal.

5.1 On-Off Keying (OOK)

To transmit information *via* OOK there must be two different possible system states. In our system these states are distinguished as the presence or absence of a tap (which correspond to the transmission of a *one* or a *zero*, respectively). OOK was chosen

as an initial modulation due to its simplicity of implementation. To understand the achievable bitrate with OOK modulation, we need to determine what is the **Resting Period (RP)**, mathematically denoted R_p. We define R_p as the minimal time-domain spacing between two successive taps such that we can clearly distinguish both taps in the received signal. Thus to transmit b bits it takes time bR_p.

5.2 Differential Pulse Position Modulation (DPPM)

DPPM is a form of modulation where M bits are encoded by symbols determined by a single pulse being sent at one of 2^M possible times. As soon as a symbol is sent the next symbol's transmission begins immediately (thus resulting in a varying bitrate).

We chose DPPM [52] for its advantages related to our system, which are discussed in the following paragraphs. DPPM works by modulating the time at which a signal (*i.e.,* tap) is transmitted. An example of this type of modulation (oriented toward our system) is shown in Fig. 5.1 (also shown are the same bits being transmitted *via* OOK). In this example there are two bits transmitted in each symbol, and therefore a total of four symbols. Symbols are defined by how many time intervals there are between the end of the last symbol and the start of the following symbol (*i.e.,* the symbol "01" is defined by two time intervals before the signal is sent). We call the length of these time intervals the **Precision** value. Precision is defined by the minimum time-domain spacing that can occur between potential stimulus such that we can determine the exact time at which the stimulus was sent. The Precision value is directly tied to how precisely we can determine the start time of a tap in a signal where only one tap occurs. Since the time it takes to send a symbol depends on which

symbol is sent, the bit rate of this system varies depending on exactly which symbols are being transmitted. Thus, depending on the nature of the information being sent, it may be possible to further optimize this system by designing a coding scheme that prioritizes symbols leading to a higher bit rate.

Additionally, DPPM is energy efficient because only one tap is required for each symbol transmitted. A further advantage of DPPM is that it does not require a perfectly synchronized clock between the transmitter and receiver. A noteworthy drawback is that when using DPPM a single symbol error can disrupt the correct receipt of all following symbols. For this reason it is often beneficial to include a periodic synchronization sequence to compensate for possible bit errors.

Consider DPPM as paired with our proposed system. Given a precision p, a resting period R_p, and $|S|$ symbols, we want to determine how long it will take to transmit a single bit. Due to the variable bitrate in DPPM, a simple way to approximate the bitrate is to take the average of the slowest and the fastest transmission times possible.

For the time T_b required to transmit a single bit, the lower bound is

$$T_b \geq \frac{log_2(|S|)}{R_p}$$

and the upper bound is

$$T_b \leq \frac{log_s(|S|)}{R_p + P \times |S|}.$$

By taking these average of these values we obtain

$$T_{b,avg} = \frac{log_2(|S|)}{2R_p} + \frac{log_s(|S|)}{2(R_p + P \times |S|)}$$

which is the average time it takes to transmit a single bit.

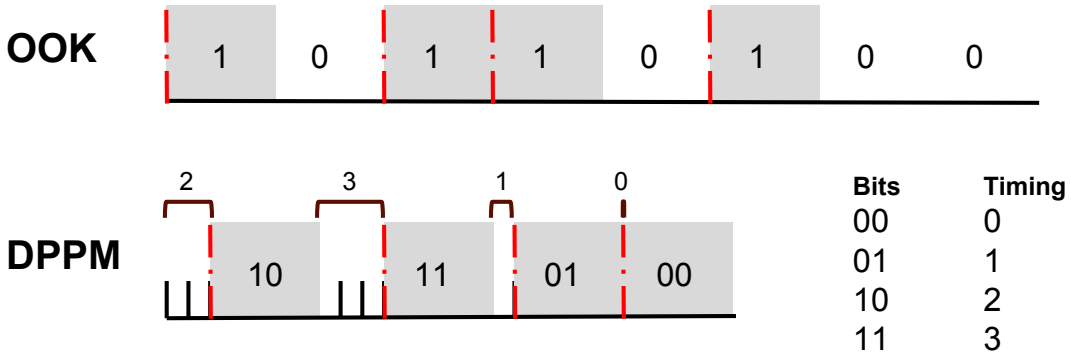

Figure 5.1: Example comparison of eight bits transmitted via OOK and DPPM

5.3 Support Vector Machine Based Demodulation

Standard SSEP analyses tend to focus on gathering many trials and averaging them in order to reduce the SNR [46], however this is deleterious to obtaining a viable bitrate for BANs. To combat this issue, we utilize a SVM binary classifer [12]. The SVM classifier works by determining an optimal hyperplane to separate binary data (in our case the presence or absence of a tactile stimulus). Figure 5.2 provides a graphical example of how this works [33]. With proper training the use of an SVM classifier can greatly reduce the amount of redundancy needed to effectively detect SSEPs [31, 40].

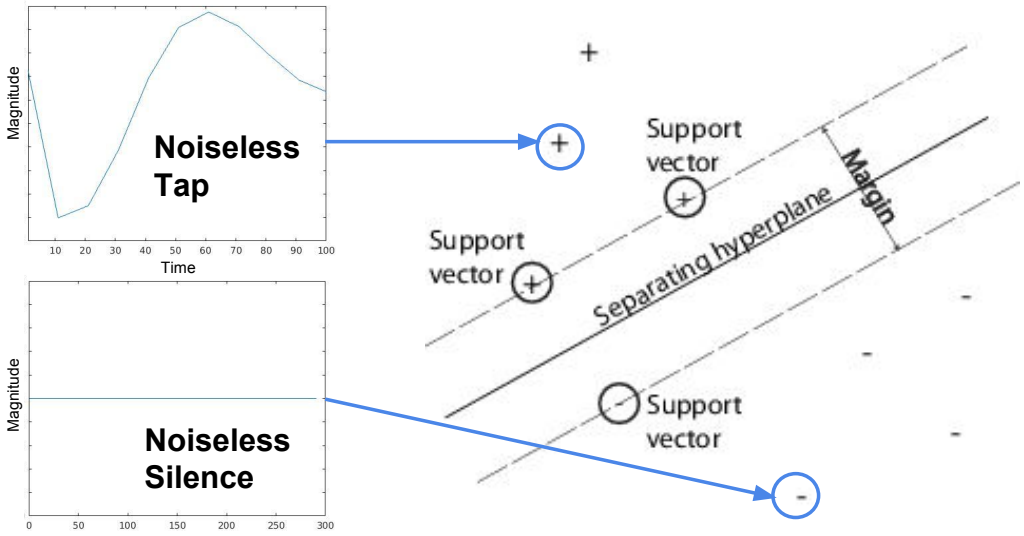

Figure 5.2: Diagram representing how an SVM classifies data.

Chapter 6

Results

In this chapter we discuss our scoring metrics, and then detail the *in-vivo* experiments using the testbed described in Chapter 3 followed by the results of our simulation code developed using the model described in Chapter 4. Finally, we consider these results in relation to each other. As with the implementation of the analytical model, all processing and results calculations were done using a combination of MATLAB and the EEGLAB toolbox.

To understand our data, we quantify the results from the classification in two ways. On one hand we use the accuracy score, defined as the ratio of correct classifications to the total number of classified samples. Mathematically this is expressed as

$$accuracy = \frac{\#p_{1,1} + \#p_{0,0}}{\#p_{1,1} + \#p_{1,0} + \#p_{0,1} + \#p_{0,0}},$$

where $\#p_{i,j}$ represents the number of occurrences of having classified the received bit as i given that the transmitted bit is j. On the other hand we used a second form of evaluation, namely, the scoring function, which represents the distance between a given sample and the decision boundary. This is done by computing the

optimal posterior probabilities using Platt's Method [43]. This is the built in scoring function provided with MATLAB's Statistics and Machine Learning Toolbox [33]. Mathematically it is defined as

$$P(y = 1|x) = \frac{1}{1 + exp(Ag(x) + B)},$$

where $g(x)$ is the classifier scores, and A and B are two scalar parameters learned by the algorithm.

6.1 Experimental Results

Using the experimental data obtained as described in Chapter 3, we sought to answer the two following questions:

1. Is there a localized source of the initial activity that occurs in the brain in response to tactile stimulation?

2. What is the shape of the waveform that appears in the EEG signal in response to this stimulation?

To answer the first question, we used the 1 Hz data collected as described in Chapter 3, and separated it into epochs, which each included a tap response. The 1 Hz data was chosen because it is the lowest tapping frequency, and thus it would be the cleanest data. As in standard in ERP detection [46] we took the average of these responses over the whole scalp, and generated the 2D activity plot shown in Fig. 6.1. This figure was generated using the built-in functions in EEGLAB [13]. In this figure, we see a distinct neural response at 60 ms on the left posterior side of the scalp. This

matches what we would expect based on the location of the somatosensory cortex, as well as the timing of the initial neural response.

After localizing the neural response, we were able to determine the electrode closest to the center of activity, which provides an answer to the second question. In Fig. 6.2, we show the voltage signal $V_{\mathrm{EEG},e}(t)$ for an electrode included in the set $\mathcal{G}$ averaged across different numbers of epochs to suppress the noise (variability among epochs), and reveal the aforementioned standard pattern within the first 100 ms from the occurrence of a tap [39, 42]. This is shown in Figure 6.2 where, as more epochs are averaged together, a distinct pattern emerges, which can be described in terms of positive and negative peaks identified with P or N respectively, as well as a number which represents their occurrence time in ms. In Figure 6.2 we see an N20 or N25, and a P55, P60, or P65, depending on the number of averaged epochs. While the shape varies slightly between sums of trials, there is a consistent pattern that repeats during the period of interest (0-100 ms). When we compare the shape of the line between 20-100 ms and the shape of the lines thereafter (100+ ms) there is no longer a common pattern between different curves. We show this data over a 100 ms epoch in Fig. 6.4 alongside analytically generated data described in the next section. Additionally, in Fig. 6.5 we show data generated in the same way but displaying the averaged response when there is no tap stimulus.

With this information, we are able to study the remainder of the simulation-based data to determine how effectively we can receive taps amidst higher transmission frequencies, as well as to better understand achievable bit rates. For this purpose we consider two key parameters from Chapter 5, *i.e., Resting Period and Precision.*

In order to determine the RP for our data, we took the data collected at different frequencies (1Hz,10Hz,100Hz) and trained SVM classifiers for each setting. We equalized the training set sizes in each setting to prevent biased results from over-training

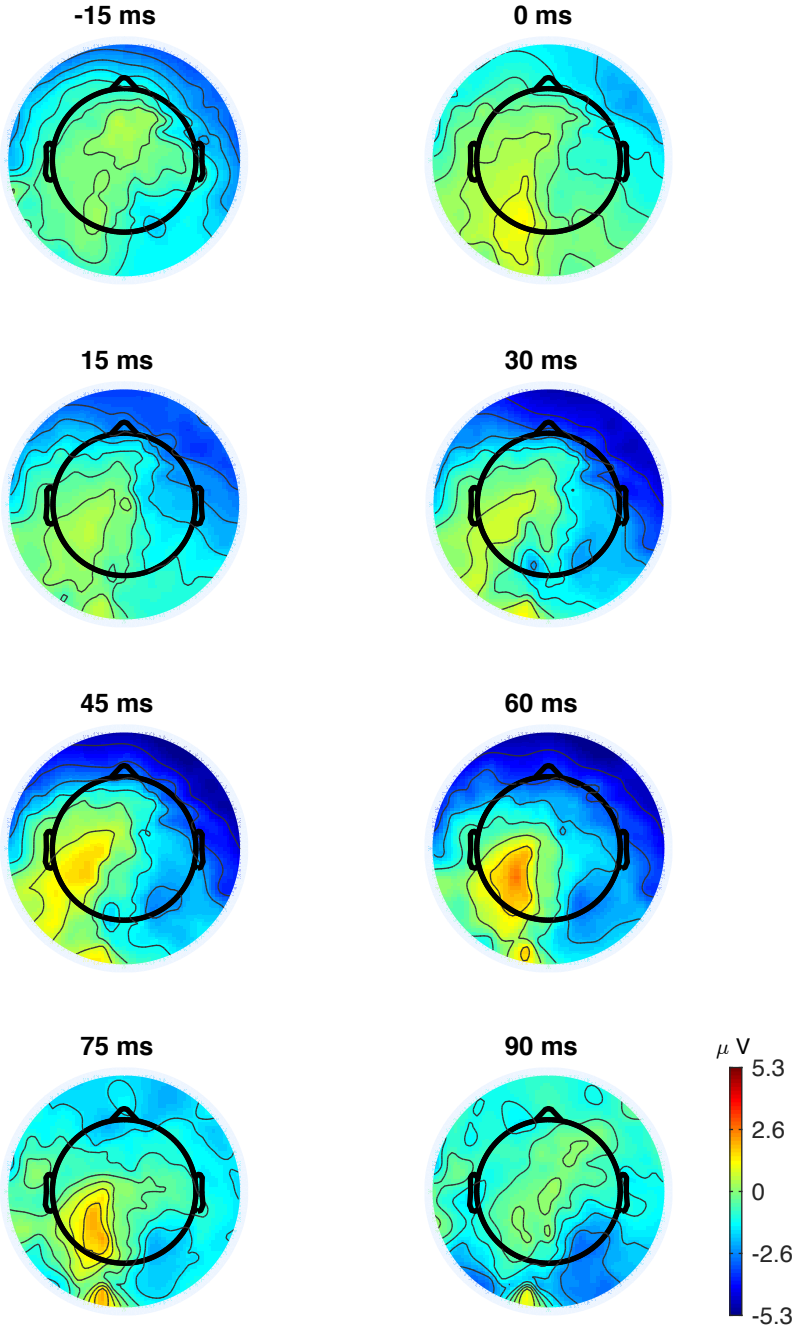

Figure 6.1: Values of the $V_{\mathrm{EEG},k}(t_p)$, $k = 1, ..., 256$, over time -15 to 90 ms averaged after stimulus onset, and spatially smoothed with respect to the standard coordinate $\vec{r}_k$ for each electrode.

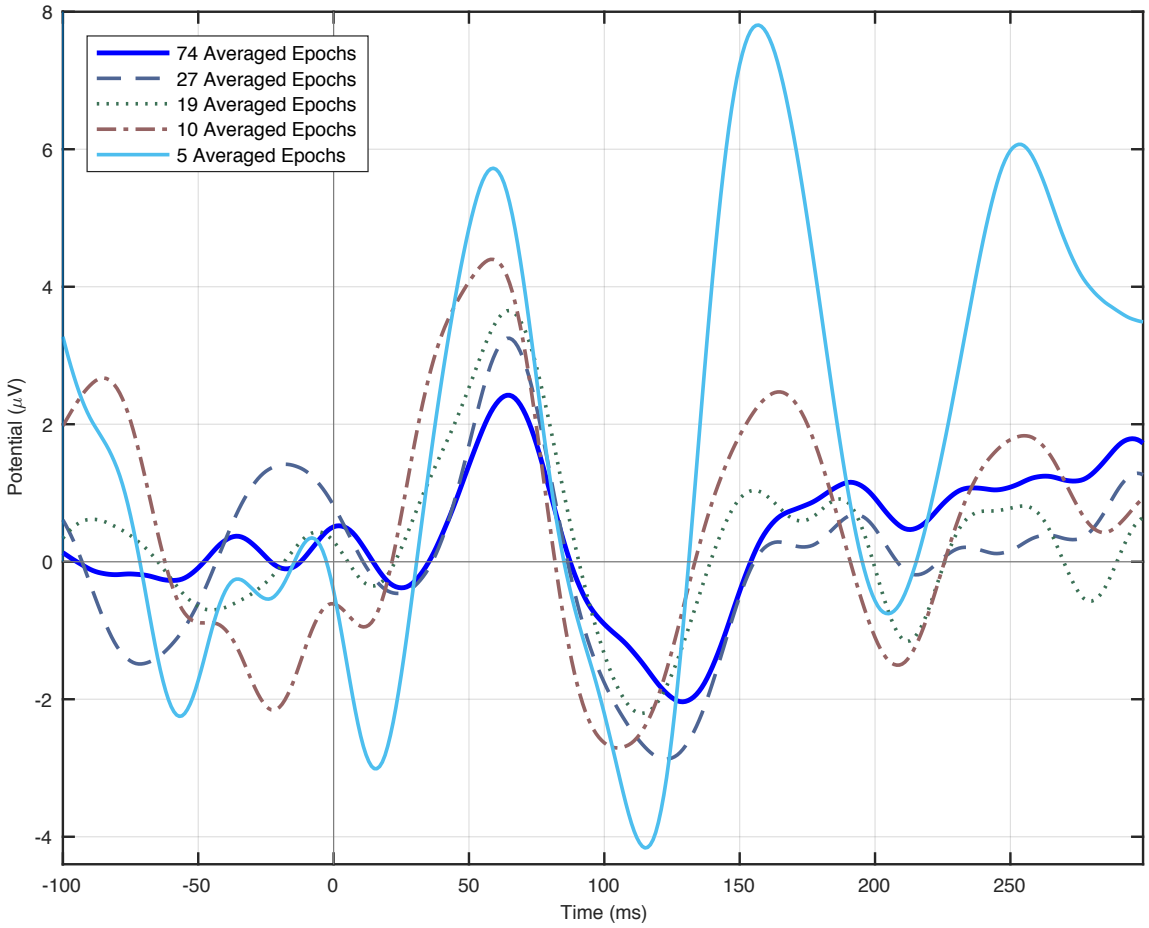

Figure 6.2: The averaged $V_{\mathrm{EEG},e}(t)$ for an electrode e included in the set $\mathcal{G}$ across different numbers of epochs. The tactile tap starts at $t_0 = 0$ ms and lasts for $T = 1$ ms, as defined in (2.1).

where more experimental data was available (particularly in the 100Hz setting). The results are shown in Fig. 6.8 alongside the related simulation-based data, which is described in the following section.

To determine precision, we used the 1 Hz and 10 Hz data, trimmed in order to only contain a single tap in any given sample. Each of these samples was then cut into segments according to "possible" tap times (more segments for testing smaller precision values), and then divided into labeled testing and training data. We sorted the results according to which values of precision were tested and they are reported

in Fig. 6.9 alongside the related simulation-based data described in the next section.

6.2 Simulation-based Results

Numerical results are obtained from the analytical framework through a MATLAB® software implementation of the models presented, and implemented according to the psuedocode presented in Chapter 4. In addition, to comply with the experimental data collection detailed in Chapter 3, we estimated the location of the center of the cortical patch area with respect to the standard EEG electrode locations [25] by computing the centroid of the magnitude of the voltage signals $V_{\mathrm{EEG},k}(t)$, where $\vec{r}_k$ is the location of the EEG electrode k for $k = 1, ..., 256$ at the time t_p of the maximum of the SSEP signal, as follows:

$$\vec{r}_{cent} = \frac{1}{256} \sum_{k=1}^{256} V_{\mathrm{EEG},k}(t_p) \vec{r}_k \, . \tag{6.1}$$

In Fig. 6.1 we show a space-smoothed (*i.e.,* the magnitude values in between the electrodes are approximated by the EEGLAB software to generate a continuous image) EEG electrode output over time -15 to 90 ms where 0 ms corresponds to stimulus onset. In agreement with the literature [39, 42], the time t_p of the maximum occurs at around 60 ms, which is the value we use to compute (2.2). The center of the aforementioned cortical patch area is set to $\vec{r}_{cent}$, as shown in Fig. 6.3.

6.2.1 Validation with Experimental Results

In order to validate our analytical model in relation to the experimental data we developed a MATLAB script using the equations provided in Chapter 4 and the associated parameters, which are summarized in Table 4.3 [16, 5]. Using this model,

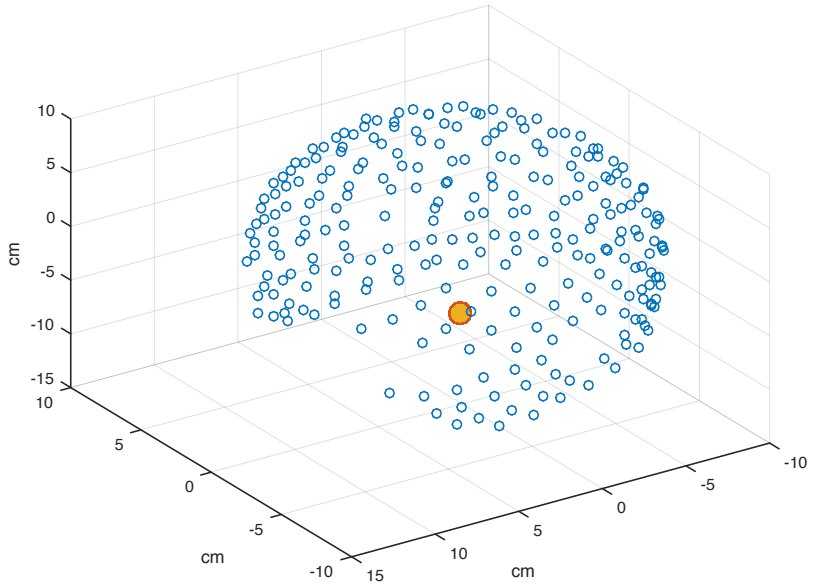

Figure 6.3: Plot of the location $\vec{r}_{cent}$ of the center of cortical patch area (larger dot) with respect to the standard EEG electrode locations $\vec{r}_k$, $k = 1, ..., 256$.

we produced 12,600 seconds of simulated EEG data corresponding to frequencies between 10 and 100 Hz.

For each test, we produced a pseudo-random sequence of bits, which determined whether the simulation would simulate a tactile tap (or not) at each time slot. This simulation produces essentially noiseless data, the only impairment occurring inherently caused by inter-symbol interference (See Fig. 6.2.1). For our study, we are interested in the somatosensory cortex activity that is localized to a specific part of the brain (the post-central gyrus), and so even in clinical settings we need only at most a few electrodes to record the related voltage signals. For this reason, as well as for computational simplicity, we only considered a single EEG electrode in our simulations.

In Figure 6.4, we show a comparison between simulated and experimental numerical values of the signal $V_{\mathrm{EEG},k}(t)$ for the electrode $e = 78$, which is at the closest location $\vec{r}_{78}$ to the centroid $\vec{r}_{cent}$ computed through (2.2), after a tap occurring at

time 0. The experimental data curve is obtained by averaging the signal $V_{\mathrm{EEG},e}(t)$ across the maximum number of available epochs, which is 74, as shown in Figure 6.2. To obtain the simulated curve in the figure, we estimated the parameter k_v defined in Section 4.4 of the results from matching values for the positive and negative peaks of the pattern shown by simulated data with those of the experimental data. In this way, we were able to obtain a reliable estimate of how membrane cortex activity $u(\mathbf{P}\vec{r}, t)$ converts into the electrical potential of the cell membrane that feeds the dipole layer model of the EEG generator, as explained in Section 4.4. By visually inspecting the figure, it is evident that the experimental and simulated curve follow a similar pattern of positive and negative peaks, which is also in agreement with the literature on SSEP analysis [39, 42]. While we record an N25 and P65 for the experimental curve, the simulated curve shows an N20 and P60. We believe these small differences in the timing of the SSEP peaks are due to the subject-to-subject variability in the processes represented by the parameters we defined in the analytical models, which have been estimated as averages.

In Fig. 6.5, we show a similar comparison between simulated and experimental numerical values as above, this time when no tap occurs, for the same electrode $e = 78$. To obtain the experimental data curve, epochs have been collected from the EEG recorded data from 100 ms before the occurrence of a tap, with a tap repetition frequency $f_t = 1$Hz, defined in Sec. 3.3. As a consequence, the recorded cortex activity had at least a time interval of 800 ms without receiving a tap-related somatosensory signal from the index finger pad. The simulated curve shows a constant value equal to 0 that is given by mechanoreceptor responses $s_i(t) = 0$ (Sec. 4.1) at any time t, somatosensory signal $I(\vec{x}_n, t) = 0$ (Sec. 4.2) at every location $\vec{x}_n$ of the receptive field, and at any time t, cortex activity $u(\vec{x}, t) = 0$ at every location $\vec{x}$ (Sec. 4.3) of the cortex patch at any time t, and finally EEG voltage signals $V_{\mathrm{EEG},78}(t) = 0$

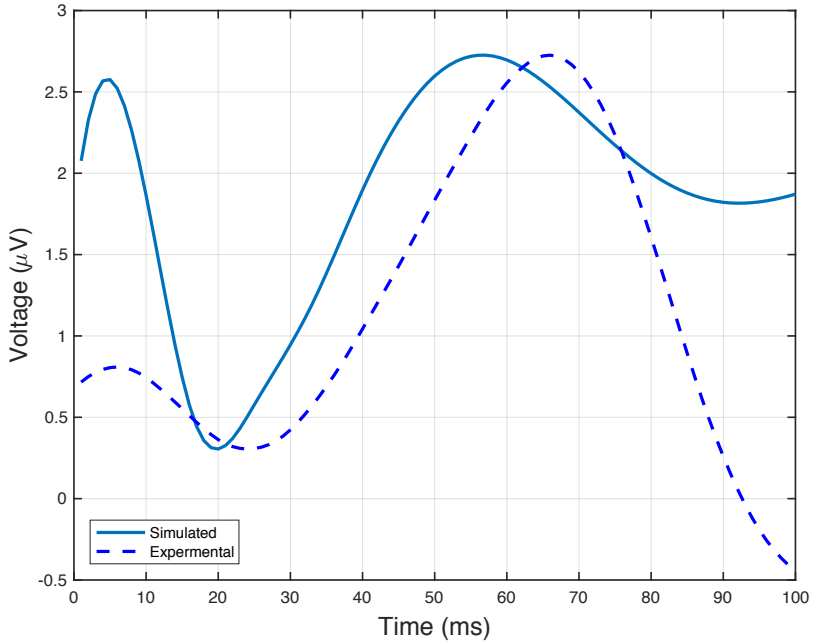

Figure 6.4: Plot of the simulated and experimental numerical values of the signal $V_{\mathrm{EEG},e}(t)$ for the electrode $e = 78$, occurring after a tap at time 0.

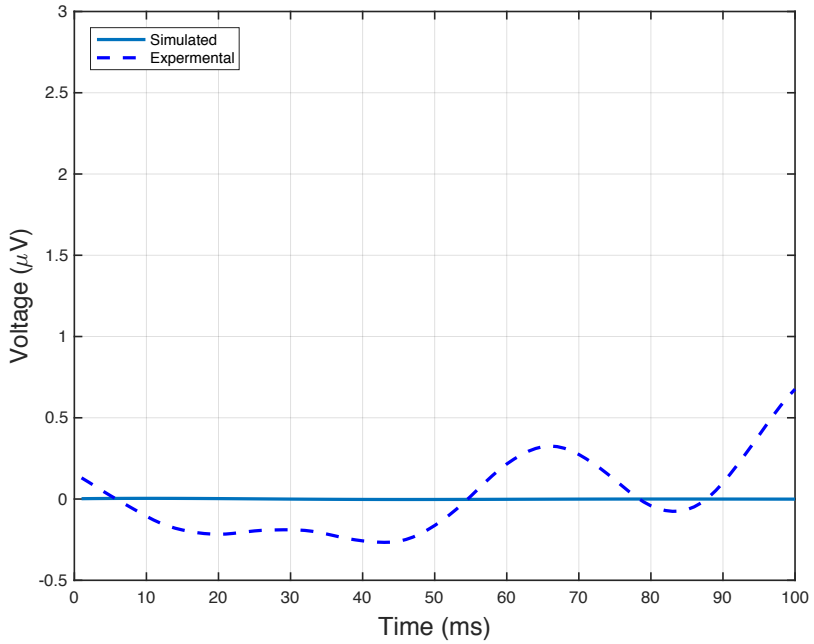

Figure 6.5: Plot of the simulated and experimental numerical values of the signal $V_{\mathrm{EEG},e}(t)$ for the electrode $e = 78$ when no tap occurs for at least 800 ms.

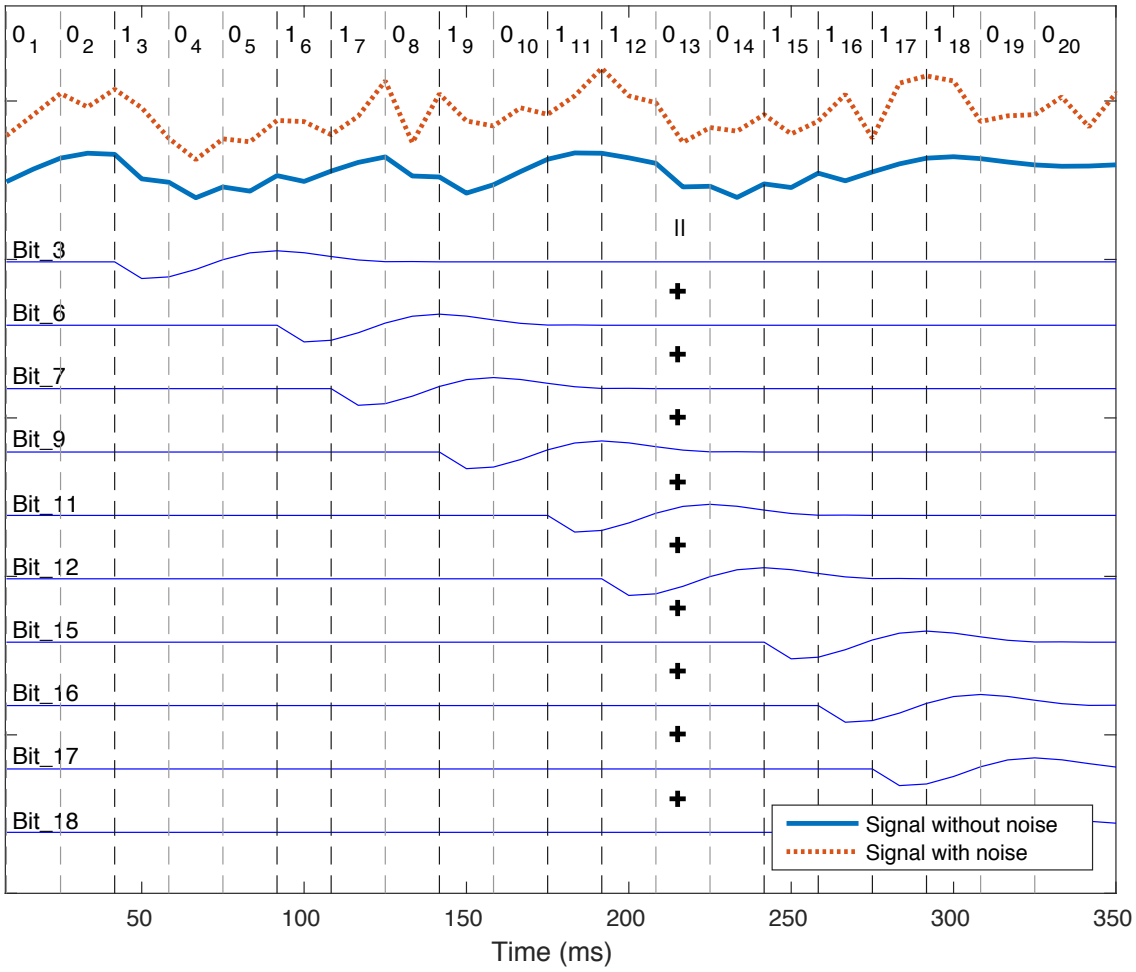

Figure 6.6: Example of simulated data. From upper to lower, we show a pseudo-random sequence of bits to be transmitted, each bit with the corresponding slot sequence number, the resulting EEG signal output from the haptic information transmission system in the case without noise, and with noise, and the decomposition of individual contributions, one for each bit, that make up the signal.

(Sec. 4.4). From Fig. 6.5, we notice that the experimental curve show values different from 0, but at the same time these voltage oscillations do not follow the common SSEP pattern [39, 42], and have attenuated maxima and minima with respect to the peaks shown in Fig. 6.4.

6.2.2 Noise Modeling

In order to probe the capacity of our system in the presence of noise, we utilized one of the most simple and commonly used noise models, the Additive White Gaussian Noise (AWGN) model. Through this model, we consider the noise to be uncorrelated and parameterized by diagonal elements made up of the EEG sensor variances [24]. In order to determine a baseline for the Signal-to-Noise Ratio (SNR) in our signal, we used the built-in MATLAB SNR function [33] to compare the experimental data in pre-stimulus and post-stimulus periods. The SNR value evaluated from this was 0.56, which was then used to determine the power-level of additive noise used in the following sections.

6.2.3 Parameters for DPPM

In order to test modulation parameters with our data, we developed a data analysis pipeline which is provided in Figure 6.7. The data pipeline consists of three primary blocks: data generation, training, and testing. Bits inputted to the data generation block are modulated, and then real or simulated EEG data is generated. The resulting labels and data are accumulated and then distributed into training and testing sets. The training data is then used to train an SVM classifier, which is used in the testing block to determine labels for the testing data and determine accuracy scores.

Using our analytical model, we generated simulation-based results by running our code that implements the analytical models detailed in Chapter 4. To match the experimental data, we captured a series of taps at constant frequencies of 1Hz, 10Hz, and 100Hz. We utilized the same procedure described in Section 6.1. We show the results for the RP and Precision values in Figures 6.8 and 6.9, respectively, and present a quantitative comparison of the data in terms of mean and standard

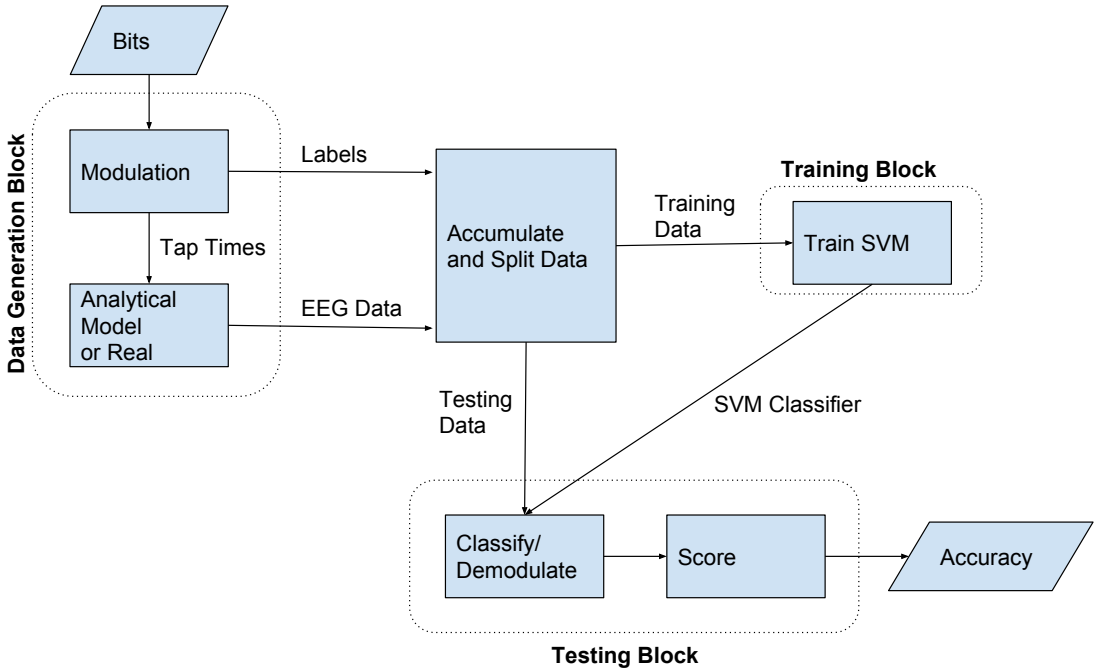

Figure 6.7: Flow chart of data collection and analysis.

deviation in Table 6.1. One issue that comes with the experimental data is a limited training set. In order to manage this issue, we similarly restricted the training set size of the analytically generated data. This is quite possibly the reason that there is little variation in the accuracy when considering different conditions in both the experimental and analytical data. That said, seeing agreement in the analytical and experimental results serves as further validation that our model is effectively modeling the experimental conditions.

Table 6.1: Mean and standard deviation of resting period and precision Results

	Mean	**Standard Dev.**
An. RP	0.7578	0.0424
Ex. RP	0.7366	0.0441
An. Prec.	0.7712	0.0476
Ex. Prec.	0.7870	0.0176

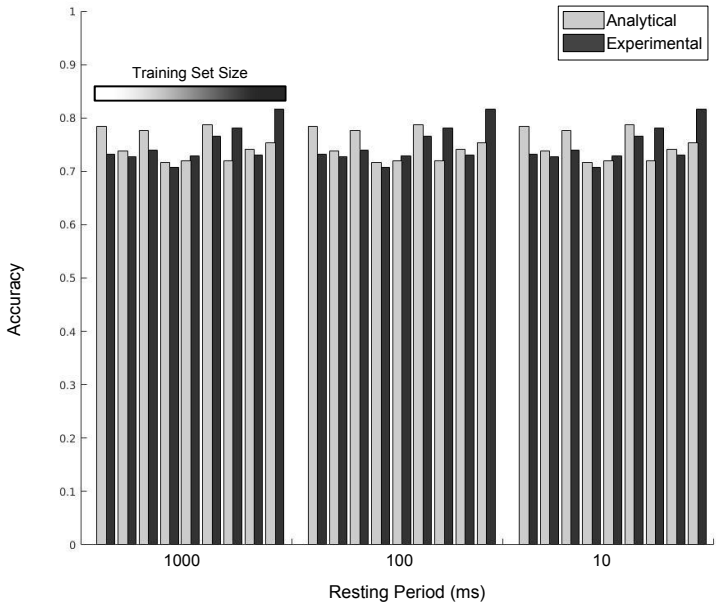

Figure 6.8: Comparison of the analytically modeled and experimentally collected results for Resting Period.

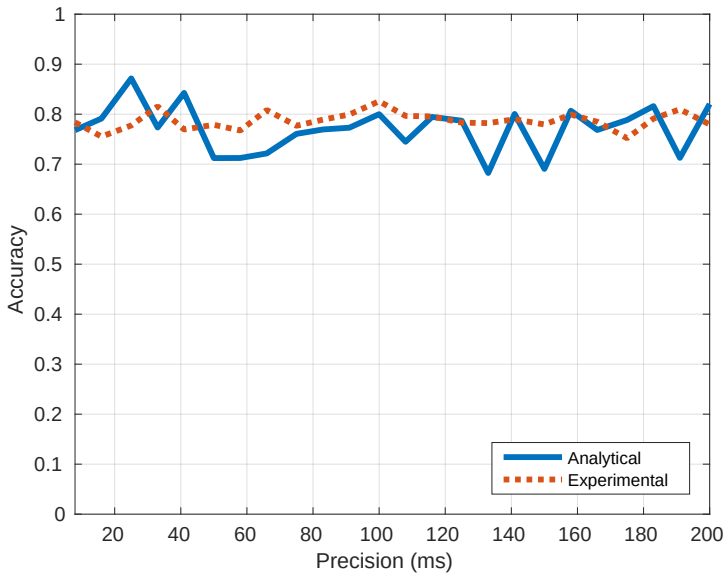

Figure 6.9: Comparison of the analytically modeled and experimentally collected results for Precision.

The value of comparing the experimental and analytical results is two-fold. On one hand, it is necessary to validate our analytical model by comparing similarities

between the experimental results and our analytical results. On the other hand, with a validated model we can effectively propose parameters for implementing these systems *in-vivo*, thus saving time and resources for conducting further experiments.

6.2.4 Analytical Comparison of OOK and DPPM

To evaluate the performance of the system through the analytical model described in Chapter 4, we separated the simulated EEG data into 39,100 epochs. The epoch length corresponds to the length of each OOK time slot, and its inverse is the bit rate (*e.g.* for a transmission frequency of 10 bits per second, the continuous EEG signal is chopped into lengths of 100 ms each), and each epoch contains either a tap stimulus or a silence period. After this preprocessing, we utilize the obtained epochs in combination with an SVM classifier (as explained in Section 5.3). The results are summarized in Figure 6.10. In order to get a reliable accuracy score, we averaged the results of 10 SVM classification scenarios for each bit rate, where each scenario included using different collections of training and testing data. We used a constant training data set of 5000 samples for each test (*e.g.* for 10 Hz data we would have a training set consisting of 5000 epochs of 100 ms long each).

We generated similar data using DPPM with our analytical model. In particular we generated 200,000 seconds of EEG data testing different DPPM values for Precision (varying from 8 ms to 34 ms) and values for the number of symbols used (between 2 and 32). To determine the bitrate for any of these settings we used the average bit rate as provided in Chapter 2, since with DPPM the bitrate is always variable.

For both OOK and DPPM we see a decrease in accuracy as the bitrate increases, and in both cases the highest accuracy occurs in the range of 30-40 bps. In addition, we see that the scores for demodulation with DPPM are less than those for OOK. This

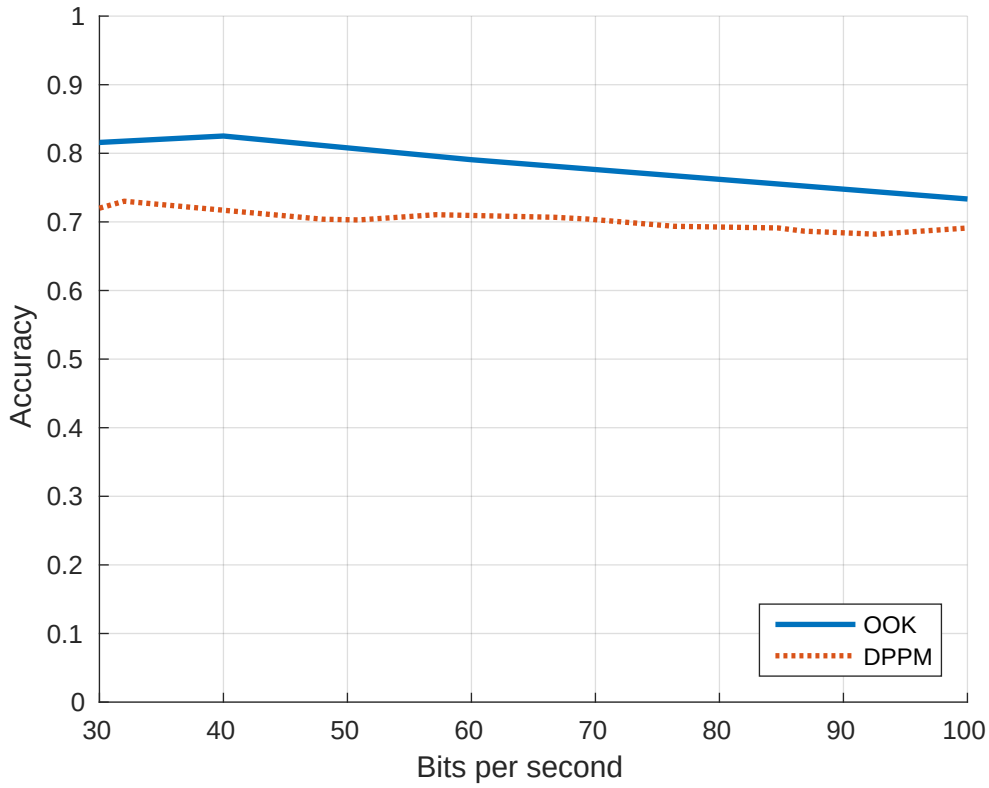

Figure 6.10: Comparison of accuracy by bit rate of analytically generated data for OOK and DPPM.

is likely due to the fact that DPPM is inherently more complex than OOK. In addition, situations in DPPM such as the number of possible symbols dramatically increase the possibility of incorrect symbol determination. For this reason it is highly beneficial to explore further techniques of effective noise reduction in EEG signals, as well as enhanced error-reduction modulation techniques such as bit redundancy. Although these bit rates are much lower than those normally required for the interconnection of wearable devices, we believe this work can serve as a proof-of-concept for further research and more advanced implementations.

Chapter 7

Conclusion

In this thesis, we proposed a communication system based on the propagation of tactile stimuli through the nervous system and its components. This system is motivated by the ever increasing number of wearable and implantable devices that demand novel sustainable solutions to realize their connectivity. We have laid the ground work for exploring the human somatosensory system as a medium to realize IBC for BANs.

In particular, this system is based on an information-transmitting tactile stimulation, realized at the index finger pad, its propagation along the nerves of somatosensory system, and the reception of the resulting somatosensory cortex activity through an EEG device. The non-invasive nature and the availability of well-established techniques for EEG signal acquisition and analysis, as well as previous neuroscience literature on the modeling of somatosensory system processes, makes this an ideal system to study for the secure and noninvasive interconnection of wearable devices.

We detailed an analytical modeling framework that captures the main physiological processes at the basis of the proposed communication system by coupling computational models of somatosensory receptive fields with mathematical expressions of the brain cortical dynamics. At the same time, we investigated the feasibility

of the proposed system through an ad-hoc experimental testbed, which also serves to validate the ability of the proposed analytical models to serve as fundamental tools for the design of systems based on haptic information transmission. We demonstrated simulation-based bitrates of around 30-40 bps, a value that may be improved with more advanced EEG noise removal as well optimization of the machine learning techniques used in demodulation.

Future work will be focused further investigation on the noise sources affecting the received signal as well as more complex noise modeling. In addition, it is necessary to explore factors such as brain plasticity and issues associated with desensitization of cutaneous receptors due to constant stimulus, which may present an issue for consumer implementations of this system.

Appendix A

List of Definitions

Accuracy The ratio of correctly classified instances to all instances classified. Mathematically equivalent to one minus the bit error rate.

Differential Pulse Position Modulation (DPPM) A type of digital modulation where the encoding of M bits is determined by a single pulse being sent at 2^M possible times.

Dorsal Column Medial Lemniscal (DCML) Pathway The DCML is a key pathway in the nervous system which transmits information related to touch from the skin and joints to postcentral gyrus of the brain.

ElectroEncephaloGram (EEG) A method of monitoring electrophysiological data in the brain.

Epoching A process through which continuous signal data is cut into numerous constant length segments.

Evoked Poential (EP) An electric response in the nervous system following the presentation of a stimulus.

N or P and a number (e.g. N20,P60) A standard in the neuroscience community for describing features on plots of EPs. N or P refers to whether the feature is a local minima or maxima respectively, and the number represents the location in time (following the related stimulus).

Neural Field Theory Uses tissue-levels models to describe the spatiotemporal characteristics of variables such as the synapse firing rate and membrane potentials.

On Off Keying (OOK) A type of digital modulation characterized by distinguishing between two states (*e.g., the presence or absence of a stimulus*) in order to transmit binary data.

Precision The minimum time-domain spacing that can occur between *potential* stimulus locations such that the original stimulus time can be effectively determined.

Resting Period (RP) The minimum time-domain spacing between two consecutive taps such that both taps are clearly distinguishable.

Somatosensory Evoked Potential (SSEP) An SSEP is an EP caused by a physical stimulus which can be detected through EEG readings. SSEP tests are often used clinically for detection of the speed of information travel across the spinal cord.

Support Vector Machine (SVM) A type of binary data classifier which develops a hyperplane from training data in order to classify testing data into one of two categories.

Bibliography

[1] "IEEE Standard for Local and metropolitan area networks - Part 15.6: Wireless Body Area Networks," *IEEE Std. 802.15.6-2012*, 2012.

[2] I. F. Akyildiz and J. M. Jornet, "The internet of nano-things," *IEEE Wireless Communications*, vol. 17, no. 6, pp. 58–63, December 2010.

[3] I. F. Akyildiz, M. Pierobon, S. Balasubramaniam, and Y. Koucheryavy, "The internet of bio-nano things," *IEEE Communications Magazine*, vol. 53, no. 3, pp. 32–40, March 2015.

[4] S. Andreescu and O. A. Sadik, "Trends and challenges in biochemical sensors for clinical and environmental monitoring," *Pure Appl. Chem.*, vol. 76, no. 4, pp. 861–878, 2004.

[5] L. Avitan, M. Teicher, and M. Abeles, "EEG generator–a model of potentials in a volume conductor," *Journal of Neurophysiology*, vol. 102, pp. 3046–3059, 2009.

[6] S. Balasubramaniam, N. T. Boyle, A. Della-Chiesa, F. Walsh, A. Mardinoglu, D. Botvich, and A. Prina-Mello, "Development of artificial neuronal networks for molecular communication," *Nano Communication Networks*, vol. 2, no. 2-3, pp. 150–160, June 2011.

[7] E. Balevi and O. Akan, "A physical channel model for nanoscale neuro-spike communications," *IEEE Transactions on Communications*, vol. PP, no. 61, p. 3, January 2013.

[8] S. Banerjee and A. Roy, *Linear Algebra and Matrix Analysis for Statistics*. Chapman and Hall/CRC, 2014.

[9] E. E. Benarroch, *Basic Neurosciences with Clinical Applications*. Elsevier, 2006.

[10] A. S. Cacciapuoti and M. Caleffi, "Receiver design for a bionic nervous system: Modeling the dendritic processing power," *IEEE Internet of Things Journal*, vol. PP, no. 99, p. 1, June 2015.

[11] S. Coombes, P. beim Graben, R. Potthast, and J. Wright, *Neural Fields: Theory and Applications*. Springer, 2014.

[12] C. Cortes and V. Vapnik, "Support-vector networks," *Machine Learning*, vol. 20, no. 3, pp. 273–297, September 1995.

[13] A. Delorme and S. Makeig, "EEGLAB: an open source toolbox for analysis of single-trial EEG dynamics," *Journal of Neuroscience Methods*, vol. 134, pp. 9–21, 2004.

[14] A. Delorme, T. Sejnowski, and S. Makeig, "Enhanced detection of artifacts in EEG data using higher-order statistics and independent component analysis," *NeuroImage*, vol. 34, no. 4, pp. 1443–1449, 2007.

[15] G. I. Detorakis and N. P. Rougier, "A neural field model of the somatosensory cortex: Formation, maintenance and reorganization of ordered topographic maps," *PLoS ONE*, vol. 7, no. 7, 2012.

[16] ——, "Structure of receptive fields in a computational model of area 3b of primary sensory cortex," *Frontiers in Computational Neuroscience*, vol. 8, no. 76, 2014.

[17] D. Durand, P. Yoo, and Z. Lertmanorat, "Neural interfacing with the peripheral nervous system," *Conf Proc IEEE Eng Med Biol Soc.*, vol. 7, pp. 5329–32, 2004.

[18] S. Geyer, A. Schleicher, and K. Zilles, "Areas 3a, 3b, and 1 of human primary somatosensory cortex," *Neuroimage*, vol. 10, no. 1, pp. 63–83, 1999.

[19] V. Glyn, V. K. Lim, J. P. Hamm, A. Mathur, and B. Hughes, "Behavioural and electrophysiological effects related to semantic violations during braille reading," *Neuropsychologia*, vol. 77, pp. 298–312, September 2015.

[20] A. Goodwin, A. Browning, and H. Wheat, "Representation of curved surfaces in responses of mechanoreceptive afferent fibers innervating the monkeys fingerpad," *The Journal of Neuroscience*, vol. 15, pp. 798–810, 1995.

[21] R. Hahnloser, H. Seung, and J. Slotine, "Permitted and forbidden sets in symmetric threshold-linear networks," *Neural Computation*, vol. 15, pp. 621–638, 2003.

[22] N. Hanisch and M. Pierobon, "Digital modulation and achievable information rates of thru-body haptic communications," in *Proc. of SPIE 10206 Disruptive Technologies in Sensors and Sensor Systems*, vol. 1020603, May 2017.

[23] R. S. Johansson and J. R. Flanagan, "Coding and use of tactile signals from the fingertips in object manipulation tasks," *Nature Reviews Neuroscience*, vol. 10, pp. 345–359, May 2009.

[24] S. C. Jun, S. M. Plis, D. M. Ranken, and D. M. Schmidt, "Spatiotemporal noise covariance estimation from limited empirical magnetoencephalographic data," *Physics in Medicine and Biology*, vol. 51, pp. 5549–5564, 2006.

[25] V. Jurcak, D. Tsuzuki, and I. Dan, "10/20, 10/10, and 10/5 systems revisited: their validity as relative head-surface-based positioning systems," *Neuroimage*, vol. 34, pp. 1600–11, 2007.

[26] K. L. Karanam and M. Gotlur, "Body area networks," *International Journal of Research in Engineering and Technology*, vol. 5, pp. 1–8, 2016.

[27] A. Khodaei and M. Pierobon, "An intra-body linear channel model based on neuronal subthreshold stimulation," in *Proc. of the 2016 IEEE International Conference on Communications (ICC)*, Kuala Lumpur, Malaysia, May 2016.

[28] ——, "Subthreshold linear modeling of dendritic trees: A computational approach," in *Proc. of the 2016 International Conference of IEEE in Medicine and Biology Society (EMBC)*, Orlando, FA, USA, August 2016.

[29] B. Kibret, M. Seyed, D. Lai, and M. Faulkner, "Investigation of galvanic-coupled intrabody communication using the human body circuit model," *IEEE Journal of Biomedical and Health Informatics*, vol. 18, no. 4, pp. 2168–2194, July 2014.

[30] S. Kota, L. Gupta, D. Molfese, and R. Vaidyanathan, "A dynamic channel selection strategy for dense array ERP classification," *IEEE Transactions on Biomedical Engineering*, vol. 56, no. 4, pp. 1040–1051, 2009.

[31] T. Lan, C. Huang, and D. Erdogmus, "A comparison of temporal windowing schemes for single-trial ERP detection," *4th International IEEE/EMBS Conference on Neural Engineering*, 2009.

[32] D. Malak and O. B. Akan, "Molecular communication nanonetworks inside human body," *Nano Communication Networks*, vol. 3, no. 1, pp. 19–35, March 2012.

[33] MATLAB, *version 8.6.0 (R2015b)*. Natick, Massachusetts: The MathWorks Inc., 2015.

[34] F. Mesiti and I. Balasingham, "Nanomachine-to-neuron communication interfaces for neuronal stimulation at nanoscale," *IEEE Transactions on Communications*, vol. 31, no. 12, pp. 695–704, December 2013.

[35] S. Micera and X. Navarro, "Bidirectional interfaces with the peripheral nervous system," *Int Rev Neurobiol.*, vol. 86, pp. 23–38, 2009.

[36] S. Movassaghi, M.Abolhasan, J. Lipman, D. Smith, and A. Jamalipour, "Wireless body area networks: A survey," *Communications Surveys & Tutorials, IEEE*, vol. 16, no. 3, pp. 1658–1686, January 2014.

[37] A. Nakamura, T. Yamada, A. Goto, T. Kato, K. Ito, Y. Abe, T. Kachi, , and R. Kakigi, "Somatosensory homunculus as drawn by meg," *Neuroimage*, vol. 7, pp. 377–386, 1998.

[38] P. L. Nunez and R. Srinivasan, *Electric Fields of the Brain: The Neurophysics of EEG, 2nd Edition*. Oxford University Press, 2006.

[39] M. Nuwer, "Fundamentals of evoked potentials and common clinical applications today," *Electroencephalography and Clinical Neurophysiology*, vol. 106, pp. 170–183, 1998.

[40] H. Parvar, L. Sculthorpe-Petley, J. Satel, R. Boshra, R. C. N. DArcy, and T. P. Trappenberg, "Detection of event-related potentials in individual subjects using support vector machines," *Brain Informatics*, vol. 2, no. 1, p. 112, 2014.

[41] M. Par, A. M. Smith, and F. L. Rice, "Distribution and terminal arborizations of cutaneous mechanoreceptors in the glabrous finger pads of the monkey," *Journal of Comparative Neurology*, vol. 445, no. 4, p. 347359, 2002.

[42] S. R. Passmore, B. Murphy, and T. D. Lee, "The origin, and application of somatosensory evoked potentials as a neurophysiological technique to investigate neuroplasticity," *J Can Chiropr Assoc*, vol. 58, pp. 170–183, 2014.

[43] J. Platt, *Probabilistic outputs for support vector machines and comparisons to regularized likelihood methods.* MIT Press, 1999.

[44] D. Purves, G. J. Augustine, D. Fitzpatrick, L. C. Katz, A.-S. LaMantia, J. O. McNamara, and S. M. Williams, *Neuroscience.* Sinauer Associates, 2001.

[45] P. P. Ray, "Channel modeling of human somatosensory nanonetwork: Body discriminative touch and proprioception perspective," *International Journal on Computer Science and Engineering*, vol. 5, no. 10, pp. 874–884, 2013.

[46] A. O. Rossetti and S. Laureys, *Clinical neurophysiology in disorders of consciousness: brain function monitoring in the ICU and beyond.* Springer, 2015.

[47] G. E. Santagati and T. Melodia, "Sonar inside your body: Prototyping ultrasonic intra-body sensor networks," in *Proc. of IEEE Conference on Computer Communications (INFOCOM)*, Toronto, Canada, April 2014.

[48] ——, "Opto-ultrasonic communications for wireless intra-body nanonetworks," *Nano Communication Networks*, vol. 5, no. 1-2, pp. 3–14, March 2014.

[49] E. Sazonov and M. R. Neuman, Eds., *Wearable Sensors: Fundamentals, Implementation and Applications*. Elsevier, 2014.

[50] M. Seyedi, B. Kibret, D. T. H. Lai, and M. Faulkner, "A survey on intrabody communications for body area network applications," *IEEE Communications Magazine*, vol. 60, no. 8, pp. 2067–2079, August 2013.

[51] C. E. Shelton, Y. Luo, and Y. Shen, "Measurement and analysis of braille stimulus to brain using an EEG: A preliminary study," in *Proc. of IEEE International Conference on Cyber Technology in Automation, Control and Intelligent Systems*, Nanjing, China, May 2013.

[52] D.-S. Shiu and J. M. Kahn, "Differential pulse position modulation for power-efficient wireless infrared communication," in *IEEE GLOBECOM 1998 (Cat. NO. 98CH36250)*, vol. 1, 1998, pp. 219–224 vol.1.

[53] J. Suzuki, S. Balasubramaniam, S. Pautot, V. D. P. Meza, and Y. Koucheryavy, "A service-oriented architecture for body area nanonetworks with neuron-based molecular communication," *Mobile Netw Appl*, vol. 19, pp. 707–717, November 2014.

[54] F. Xu, Z. Qin, C. C. Tan, B. Wang, , and Q. Li, "IMDguard: Securing implantable medical devices with the external wearable guardian," in *Proc. of IEEE International Conference on Computer Communications (INFOCOM)*, April 2011.

[55] Y. Yang and C. K. Yeo, "Conceptual network model from sensory neurons to astrocytes of the human nervous system," *IEEE Transactions on Biomedical Engineering*, vol. 62, no. 7, pp. 1843–1852, 2015.